Cu, Fe, and S *K*- and *L*-edge XANES spectra of $CuFeS_2$: Localization and interpretation of pre-peak states

O. Šipr, P. Machek, and A. Šimůnek
Institute of Physics, Academy of Sciences of the Czech Republic, Cukrovarnická 10, 162 53 Praha 6, Czech Republic
(Received 18 September 2003; revised manuscript received 18 December 2003; published 28 April 2004)

The pre-peak in the x-ray-absorption near-edge structure (XANES) of $CuFeS_2$ is studied by exploring the associated photoelectron probability density as well as by investigating the cluster size effect. All significant features of the Cu, Fe, and S *K*-edge experimental spectra and of the S $L_{2,3}$-edge spectrum are successfully reproduced by the real-space multiple-scattering (RSMS) calculations with self-consistent scattering potentials and by full-potential band-structure calculations employing all-electron pseudopotentials. Pre-peak-forming photoelectron states are confined to all Fe sites of the finite cluster involved in the RSMS calculation, not just to that Fe which is the nearest one to the photoabsorbing atom. Different interpretations of the pre-peak can be unified within a single scheme of the photoelectron probability density. In order to achieve a comprehensive understanding of XANES features, both the photoelectron probability density and the cluster size effect ought to be analyzed.

DOI: 10.1103/PhysRevB.69.155115 PACS number(s): 71.20.Nr, 78.70.Dm

I. INTRODUCTION

X-ray-absorption spectroscopy (XAS) has developed into an important tool for investigating structural and electronic properties of solids. The origin of the extended x-ray-absorption fine structure (EXAFS) is intuitively well understood in terms of interference of scattered electron waves. This intuitively clear picture undoubtedly facilitated the broad dissemination of the EXAFS technique in investigating the structure of solids. On the other hand, a similarly simple interpretation of the x-ray-absorption near-edge structure (XANES) features is still lacking. There has been a growing interest recently in applying the XANES analysis to structural studies.[1–5] Having a deeper intuitive insight into the origin of XANES spectral features and on the associated photoelectron states would certainly help in further development at this research area.

The pre-peak or more generally the pre-edge structure plays a prominent role in interpreting XANES spectra. It has been used for both qualitative and quantitative assessment of the symmetry, coordination, and nearest-neighbor distances around the photoabsorbing site.[2,6–10] However, different frameworks and/or languages were used for its interpretation. The main distinction turns around the issue of localization of the electron states into which the photoelectron is ejected in the course of the pre-peak formation. One of the approaches is to describe these states as localized or (quasi)bound states, sometimes explicitly distinguishing them from continuum or multiple-scattering resonances.[11–14] On the other hand, another approach interprets the pre-peak states as truly delocalized multiple-scattering resonances, extended over several atomic shells.[15–18] In some papers, both frameworks are encompassed and applied for describing different pre-edge features of different compounds selectively.[19,20] It would certainly be helpful to investigate localization of pre-edge photoelectron states in a well-defined manner, enabling thus a unified interpretation of different viewpoints.

The chalcopyrite $CuFeS_2$ offers an opportunity to study the same pre-edge states viewed from three different sites, by examining the Cu, Fe, and S *K*- and *L*-edge XANES spectra. While the Cu and Fe *K* edges display modest pre-peaks, the S *K*-edge pre-peak is very intensive, approximately of the same height as the main maximum.[21,22] A mild pre-peak can be seen in the S $L_{2,3}$-edge XANES as well.[23] These pre-edge states have been described either as arising from the Fe $3d$ band hybridized with the S and/or Cu states[21–23] or from interference effects of the photoelectron wave function from the crystal structure.[24] Theoretical spectra obtained via the real-space multiple-scattering (RSMS) formalism were presented for the Cu and Fe *K*-edges,[24] however, the agreement between the theory and experiment was not very good. No other calculations of XANES of $CuFeS_2$ were published, to the authors' knowledge.

Apart from serving as a playground for studying the pre-peak in general, XANES of $CuFeS_2$ is interesting on its own as well, because it remarkably differs from spectra of its isostructural analogs. Indeed, the electronic structure and XANES spectra of ternary chalcopyrite semiconductors of the I-III-VI_2 type[22,25–28] and of ternary pnictide semiconductors of the II-IV-V_2 type[29,30] are quite similar to each other (both inside each of the groups and across them), which makes the aside-standing $CuFeS_2$ quite unique.[30] By comparing the chemical formula of these isostructural compounds, one immediately gets the idea that the reason for the distinctiveness of $CuFeS_2$ has to be the presence of a second transition-metal element Fe in the compound. However, it would be instructive to acquire a deeper insight into the mechanism through which the Fe atoms induce the pronounced changes in the XANES spectra of $CuFeS_2$ with respect to spectra of I-III-VI_2 and II-IV-V_2 compounds.

Traditionally, the role of particular atoms in forming the spectral structure has been investigated by changing the size and/or geometry of the cluster for which the spectrum is calculated within the RSMS formalism.[7,16] Such a procedure may assess the empirical importance of various atoms for creating a particular peak, however, it does not provide a

direct information about the *spatial localization* of the corresponding photoelectron states. That kind of information can be obtained by inspecting the quantum-mechanical probability density of the photoelectron ejected during the absorption of x-ray photons.[31] On the other hand, such a probability density is not directly related to creation of spectral peaks. By comparing the outcome of both analyses, one can obtain quite a comprehensive look both on the origin and on the localization of the pre-peak in XANES of $CuFeS_2$.

The purpose of this paper is thus to study XANES spectra of $CuFeS_2$, to explore the Cu, Fe, and S pre-peaks by investigating the theoretical spectra and the photoelectron probability density and to interconnect various approaches to analyzing the pre-edge structure. The paper is organized as follows: First, we outline our experimental and theoretical methods. Then we present the Cu, Fe, and S *K*-edge and S *L*-edge theoretical and experimental XANES spectra. The photoelectron probability density is presented and discussed in the following section, followed by exploration of the cluster size effect. After comparison of both approaches towards the pre-peak analysis we present our conclusions.

II. METHODOLOGICAL FRAMEWORK

A. Experiment

The Cu and Fe *K*-edge spectra of polycrystalline $CuFeS_2$ were measured using synchrotron radiation at HASYLAB, Hamburg. Both edges were recorded in the transmission mode at the A1 beamline with a Si (111) two-crystal monochromator. The energy resolution of the monochromator was about 1.2 eV at the Cu edge and 1 eV at the Fe edge. The intensities in front of and behind the sample were monitored and recorded using ionization chambers filled by 50% argon-doped nitrogen mixture. The samples were prepared by a mechanical powdering of the natural chalcopyrite and by making cellulose based pills with an appropriate amount of the powder.

Experimental S spectra were taken from other works: the S *K*-edge XANES was digitized from the paper of Sainctavit *et al.*[22] and the S $L_{2,3}$-edge XANES was digitized from the paper of Li *et al.*[23]

B. Theoretical spectra

Theoretical spectra were obtained from *ab initio* calculations in a twofold way, namely, in a real space within a RSMS framework[32,33] and in a reciprocal space within a pseudopotential formalism. The RSMS calculations were performed using the RSMS code, which is an amended descendant of the ICXANES code[34] and is maintained by our group.[35] Full multiple scattering among all atoms of model clusters was included via a matrix inversion. Self-consistent muffin-tin scattering potentials were obtained from SCF-$X\alpha$ (SCF—self-consistent field) molecular calculations[36] for clusters of 21 atoms embedded in a crystal, employing an amended XASCF code of Case and Cook.[37,38] The muffin-tin radii overlapped by 10% and were chosen according to the matching-potential condition. A screened and relaxed core hole at the photoabsorbing atom was included. An energy-independent $X\alpha$ exchange-correlation potential was employed, using the Kohn-Sham value of $\alpha = 0.66$.

Another set of theoretical spectra was obtained via a full-potential band-structure calculation based on an all-electron pseudopotential formalism and a plane-wave basis set.[38,39] The technique works with relaxed core states and provides full electron charge densities comparable with results of a full-potential linearized augmented plane-wave method (see also Ref. 40 for a comparison). The Ceperley-Adler exchange and correlation term in an analytical form[41] was used in our band-structure calculation. To obtain dipole transition-matrix elements of the core-valence transition, we split it into its radial and angular parts,

$$\langle \psi_c | \boldsymbol{\varepsilon} \boldsymbol{r} | \psi_{n\boldsymbol{k}} \rangle = \langle \psi_c | r | \psi_{n\boldsymbol{k}} \rangle_{\mathrm{rad}} \times \langle \psi_c | \frac{\boldsymbol{\varepsilon} \boldsymbol{r}}{r} | \psi_{n\boldsymbol{k}} \rangle_{\mathrm{ang}}. \qquad (1)$$

In Eq. (1), $\boldsymbol{\varepsilon}$ is the polarization vector, $\boldsymbol{k}$ is the crystal momentum, and n is the band subscript. The value of the radial part $\langle \psi_c | r | \psi_{n\boldsymbol{k}} \rangle_{\mathrm{rad}}$ is approximated by a constant in our calculation (this corresponds to a nondispersive core state and a single nondispersive valence state of a fixed energy). The angular part was evaluated using the full symmetry and dispersion of valence wave functions $\psi_{n\boldsymbol{k}}(\boldsymbol{r})$ in the $\boldsymbol{k}$ space and, thus, determines the shape of spectral peaks. A similar approach for evaluating matrix elements was used in Ref. 42.

All theoretical curves presented here were convoluted by a Lorentzian function with an energy-dependent width; its constant part accounts for the core-hole lifetime broadening,[43] the energy-dependent part accounts for the finite photoelectron lifetime according to the universal (empirical) curve.[3,44] The experimental energy resolution was simulated by an additional broadening by a Gaussian function (with a width of 1.2 eV for the Cu edge, 1.0 eV for the Fe edge, 0.6 eV for the S *K* edge, and 0.2 eV for the S $L_{2,3}$-edge).

C. Photoelectron probability density

The concept of the photoelectron probability density (PEPD) was applied for a XANES analysis in Ref. 45 for the first time and its detailed description can be found in the paper of Šipr.[31] We recall its essence only briefly here.

The x-ray-absorption fine structure arises due to the energy dependence of the core-electron photoeffect: an electron absorbs an x-ray photon, is ejected off the atom, and starts to travel inside the solid. One can thus associate a particular spectral peak with a multiple scattering of a photoelectron of a certain energy by neighboring atoms. The probability $P(\boldsymbol{r})$ that an electron ejected as a result of an absorption of a photon with energy ω can be found at position $\boldsymbol{r}$ can be evaluated as

$$P(\boldsymbol{r}) = \frac{1}{\sigma_{\mathrm{XAS}}} \int d^2\hat{\boldsymbol{k}} \frac{d\sigma}{d\Omega_{\boldsymbol{k}}} |\psi_{\boldsymbol{k}}^{(-)}(\boldsymbol{r})|^2. \qquad (2)$$

The term $d\sigma/d\Omega_{\boldsymbol{k}}$ is the photoelectron diffraction cross section, the final state $|\psi_{\boldsymbol{k}}^{(-)}\rangle$ is a solution of the Lippman-Schwinger equation

$$\psi_{\mathbf{k}}^{(-)}(\mathbf{r}) = e^{i\mathbf{k}\mathbf{r}} + \int d^3\mathbf{r}'\, G_0^{(-)}(\mathbf{r},\mathbf{r}')V(\mathbf{r}')\psi_{\mathbf{k}}^{(-)}(\mathbf{r}'), \quad (3)$$

where $G_0^{(-)}(\mathbf{r},\mathbf{r}')$ is the advanced free-electron Green function and $V(\mathbf{r}')$ describes the potential of the cluster, and the XAS cross section σ_{XAS} is

$$\sigma_{\mathrm{XAS}} = \int d^2\hat{\mathbf{k}} \frac{d\sigma}{d\Omega_{\mathbf{k}}}. \quad (4)$$

The probability density $P(\mathbf{r})$ introduced in this way is measured in ''units of free-electron probability density.'' Further equations describing how to practically evaluate $P(\mathbf{r})$ can be found in Ref. 31.

As our aim is to explore the spatial localization of pre-peak-generating states in an atomic cluster, it is sufficient to compare not the $P(\mathbf{r})$ itself but rather its averages inside suitably chosen spheres,

$$P^{(j)} \equiv \frac{1}{V^{(j)}} \int_0^{R^{(j)}} dr\, r^2 \int d^2\hat{\mathbf{r}} P(\mathbf{r}), \quad (5)$$

where $R^{(j)}$ is a suitably chosen normalization radius and $V^{(j)}$ is the volume of the normalization sphere around the jth atomic site. The average site-related probabilities $P^{(j)}$ depend only mildly on the normalization radius $R^{(j)}$ as long as it acquires ''reasonable'' values (say within 30% of the muffin-tin radius). The PEPD's $P^{(j)}$ presented in Sec. III C were obtained for $R^{(j)}$ identical with the muffin-tin radii of respective atoms.

The probability density $P(\mathbf{r})$ defined by Eq. (2) is to a large extent dominated by isotropic density of states (DOS) effects.[31,46] This contribution can be quantified by defining a DOS-like probability density $P_{\mathrm{DOS}}(\mathbf{r})$,

$$P_{\mathrm{DOS}}(\mathbf{r}) \equiv \frac{1}{4\pi} \int d^2\hat{\mathbf{k}} |\psi_{\mathbf{k}}^{(-)}(\mathbf{r})|^2 = \frac{4\pi^2}{k} n(\mathbf{r},E), \quad (6)$$

meaning that states with different $\hat{\mathbf{k}}$ contribute to $P_{\mathrm{DOS}}(\mathbf{r})$ with identical weights, just as is the case of local $\mathbf{r}$-dependent density of states.[46] Note that the factor $4\pi^2/k$ by which $P_{\mathrm{DOS}}(\mathbf{r})$ differs from $n(\mathbf{r},E)$ stems from the normalization of $P(\mathbf{r})$ to the free-electron probability density. Atomic-sphere related quantities $P_{\mathrm{DOS}}^{(j)}$ and $\Delta P_{\mathrm{DOS}}^{(j)}$ can be defined analogously to Eq. (5),

$$P_{\mathrm{DOS}}^{(j)} \equiv \frac{1}{V^{(j)}} \int_0^{R^{(j)}} dr\, r^2 \int d^2\hat{\mathbf{r}} P_{\mathrm{DOS}}(\mathbf{r}), \quad (7)$$

$$\Delta P_{\mathrm{DOS}}^{(j)} \equiv \frac{1}{V^{(j)}} \int_0^{R^{(j)}} dr\, r^2 \int d^2\hat{\mathbf{r}} [P(\mathbf{r}) - P_{\mathrm{DOS}}(\mathbf{r})], \quad (8)$$

as well as their ratio

$$q_{\mathrm{DOS}}^{(j)} \equiv \frac{P^{(j)} - P_{\mathrm{DOS}}^{(j)}}{P^{(j)}} = \frac{\Delta P_{\mathrm{DOS}}^{(j)}}{P^{(j)}}. \quad (9)$$

The differential probability density $\Delta P_{\mathrm{DOS}}^{(j)}$ informs how the spatial localization of a XANES electron differs from the spatial localization of a ''generic'' electron (with the same energy); the dimensionless relative differential probability density $q_{\mathrm{DOS}}^{(j)}$ measures this quantity relative to the site-related probability $P^{(j)}$. Roughly speaking, while $P^{(j)}$ informs about the probability that photoelectron can be found close to the jth site, $q_{\mathrm{DOS}}^{(j)}$ informs what portion of its presence is caused by specific XAS-related effects.

III. RESULTS AND DISCUSSION

A. Cu, Fe, and S *K*-edge spectra

Before analyzing the origin of $CuFeS_2$ spectral peaks and the localization of the associated photoelectron, one has to verify that our method describes the experimental XANES well enough. The experimental and theoretical Cu, Fe, and S *K*-edge XANES spectra of $CuFeS_2$ are displayed in Fig. 1. The horizontal alignment of the theoretical spectra at different edges was provided by the calculation itself, the block-wise alignment of the band-structure and the RSMS calculations as well as of the experimental spectra was performed by hand. The zero of the energy scale was set to the onset of empty states in our RSMS calculations. The vertical scales were set for each of the curves individually, so that the best agreement between the theory and experiment is achieved. Our experimental spectra at the Cu and Fe *K* edges are in a good agreement with earlier measurements of Petiau *et al.*[21] and McKeown *et al.*[24]

The RSMS calculations for clusters of 207 atoms are presented here both with and without accounting for the 1*s* core hole. We checked that a full cluster size convergence has been reached for this size of the clusters (cf. also Sec. III D below). As it can be seen from Fig. 1, the influence of the core hole is not very significant for $CuFeS_2$—at least as concerns its effectively one-particle treatment by applying the final-state rule. Its effect is most visible at the S *K* edge: it decreases the pre-peak intensity and increases the intensity at the low-energy shoulder of the main peak. The latter effect (the change in the shape of the main peak) is not surprising, as similar effects were observed for a number of other compounds as well.[47–51] On the other hand, the observed *decrease* of the pre-peak intensity caused by inclusion of the core hole is unusual. We cannot put much weight to this finding, however, as our computational scheme is not particularly suited for assessing subtle core-hole effects close to the very edge. The pre-peak intensity, namely, significantly depends on the position of the onset of the conduction band, which cannot be determined very accurately within the local-density approximation approach we employ.

Our RSMS calculations account both for dipole and for quadrupole transitions. We found that the quadrupole contribution is always at least by two orders of magnitude smaller than the dipole contribution and it can be, therefore, completely ignored in this case.

As can be seen from Fig. 1, both the RSMS and the pseudopotential calculations are quite in a good agreement with the experiment. For a more quantified comparison, we turn to the S *K* spectrum, where the spectral features are most pronounced, and compare the separations between prominent peaks as provided by the experiment and by all three calcu-

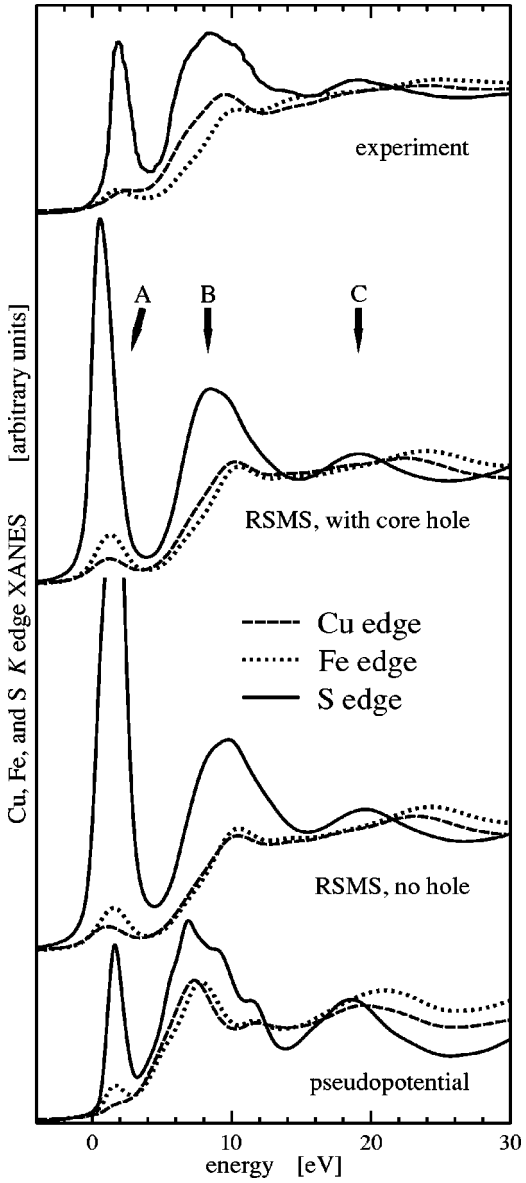

FIG. 1. Cu, Fe, and S *K*-edge XANES spectra of $CuFeS_2$ as obtained from experiment, from RSMS calculations with a 1*s* core hole included, from RSMS calculations neglecting the core hole and from pseudopotential calculations. The experimental S *K*-edge XANES was digitized from Ref. 22. Letters *A*, *B*, and *C* mark prominent peaks in the S *K*-edge spectrum.

lations. The outcome for peak *A* (located approximately at 1.5 eV in Fig. 1), peak *B* (at 9 eV), and peak *C* (at 19 eV) is summarized in Table I. Typically, the experimental peak separation falls between the results of the RSMS and the pseudopotential calculations. The difference between the two theoretical methods cannot be caused by a mere use of different exchange-correlation potentials (cf. Sec. II B); we checked that applying the Ceperley-Adler potential to the RSMS calculations resulted in spectra differing at most by 5% in peak intensities and $\lesssim 0.5$ eV in peak positions from the spectra obtained using the Kohn-Sham potential. As our RSMS calculations use self-consistent potentials and the finite dimensions of the clusters do not play any role in this

TABLE I. Separations between prominent peaks in the S *K* edge as provided by the experiment, by the RSMS calculation which accounts for the core hole, by the RSMS calculation which ignores the core hole, and by the pseudopotential calculation. First number column shows separation between peaks *A* and *B*, second number column between peaks *B* and *C*, and third number column between peaks *A* and *C* (cf. Fig. 1). All separations are in eV's.

	A-*B*	*B*-*C*	*A*-*C*
Experiment	6.5	10.7	17.2
RSMS (with core hole)	8.1	10.4	18.5
RSMS (no hole)	8.0	10.0	18.0
Pseudopotential	5.6	11.0	16.6

respect either (Sec. III D), the muffin-tin approximation involved in the RSMS technique seems to be the most plausible reason for the differences between the RSMS and pseudopotential calculations. A more thorough investigation of this issue is, however, beyond the scope of this paper.

To conclude this section, we note that both conceptually quite different theoretical methods are able to account for the observed features of the Cu, Fe, and S *K*-edge spectra of $CuFeS_2$. One can thus rely on our theoretical scheme in analyzing the pre-peak below.

B. S $L_{2,3}$-edge spectrum

The *L* spectra, if available, give access to states characterized by different angular momentum than the *K* spectra. The S $L_{2,3}$-edge XANES of $CuFeS_2$ was measured by Li *et al.*[23] As the binding energies of the S $2p_{3/2}$ and S $2p_{1/2}$ core levels are quite close to each other [in atomic S they differ by 1.1 eV (Ref. 52)], the recorded spectrum is actually a superposition of the L_3 and L_2 spectra, mutually shifted by ~ 1 eV. The experimental S $L_{2,3}$-edge spectrum digitized from Ref. 23 and our theoretical spectrum calculated by the RSMS method are shown in Fig. 2. As our calculation is a nonrelativistic one, the theoretical spectrum we present in Fig. 2 was obtained by superposing two identical spectra corresponding to the $2p$ core-electron excitation, separated by 1.1 eV in energy and weighted according to the 2:1 branching ratio between the L_3 and L_2 spectra intensities. The agreement between the theory and the experiment is satisfactory, the largest difference is the shift of the pre-peak position by ~ 1 eV, similarly as in the case of RSMS calculations at the *K* edge.

The $L_{2,3}$-edge spectra stem from transitions into empty states with two different angular momenta, namely, $\ell = 0$ and $\ell = 2$. For heavier elements, the contributions from the *s* final states can usually be neglected,[53,54] while for lighter elements the *s* states may be important.[49] In order to assess the contributions of the final *s* and *d* states in the S $L_{2,3}$ spectrum of $CuFeS_2$, we display in Fig. 3 both the total calculated spectrum as well as the spectra calculated while including either only the *s* or only the *d* channels. Note that the spectra presented in Fig. 3 correspond to a single excitation energy, i.e., no L_3 and L_2 edges superposition was made for clarity. It can be seen from Fig. 3 that the S $L_{2,3}$-edge pre-peak is

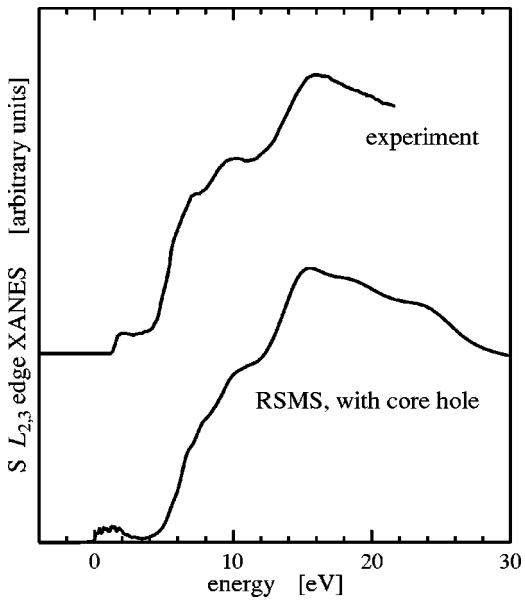

FIG. 2. The S $L_{2,3}$-edge XANES of $CuFeS_2$ as obtained from experiment (Ref. 23) and from RSMS calculations with a $2p$ core hole included.

formed by the final *s* and *d* states in approximately the same degree and that the first shoulder (around $E \approx 7$ eV in Fig. 2) is formed predominantly by the *s* states. The remaining—high-energy—part of the spectrum reflects the *d* states almost exclusively.

The core-hole effect is explored in Fig. 3, too. Similarly as in the case of the *K*-edge spectra, it is not very large. Its mostly marked consequence is an increased intensity at the low-energy end of the broad main peak (resembling an analogous effect at the S *K*-edge XANES in the preceding section). Nevertheless, even this modest effect seems to be observable in the experiment (cf. Fig. 2).

Separate *s* and *d* state contributions to the S L_3 spectrum were calculated by the pseudopotential method as well (the lowermost panel in Fig. 3). It can be seen that there is a basic agreement between the RSMS and pseudopotential results, especially as concerns the relative position of the *s* contribution with respect to peaks in the *d* curve. The differences between the peak positions provided by both types of calculation are analogous to those displayed in Table I for the *K*-edge spectrum. The too high intensity of the peak at 7 eV in the *d* state contribution provided by the pseudopotential calculation is probably caused by the neglect of the energy dependence of the radial part of the transition-matrix element [cf. Sec. II B and text below Eq. (1)]. That is also the reason why we do not display the sum of the *s* and *d* contributions in the lowermost panel of Fig. 3.

C. Probability distribution of pre-peak photoelectron states

In order to assess the localization of the photoelectron which participates in the formation of spectral peaks, we calculated the probabilities $P^{(j)}$ that it can be found in the vicinity of various atoms in a finite cluster, according to Eq. (5). As such a calculation is computationally quite demanding, we performed it mostly for clusters containing 147 atoms. We checked that the resulting XANES spectra practically do not deviate from the spectra of clusters of 207 atoms presented in Fig. 1. Additionally, in order to estimate the influence of the cluster size, we calculated the PEPD distribution solely in the pre-peak energy region for 207-atom clusters as well. All the results presented in this section were obtained for a potential which accounts for the $1s$ core hole.

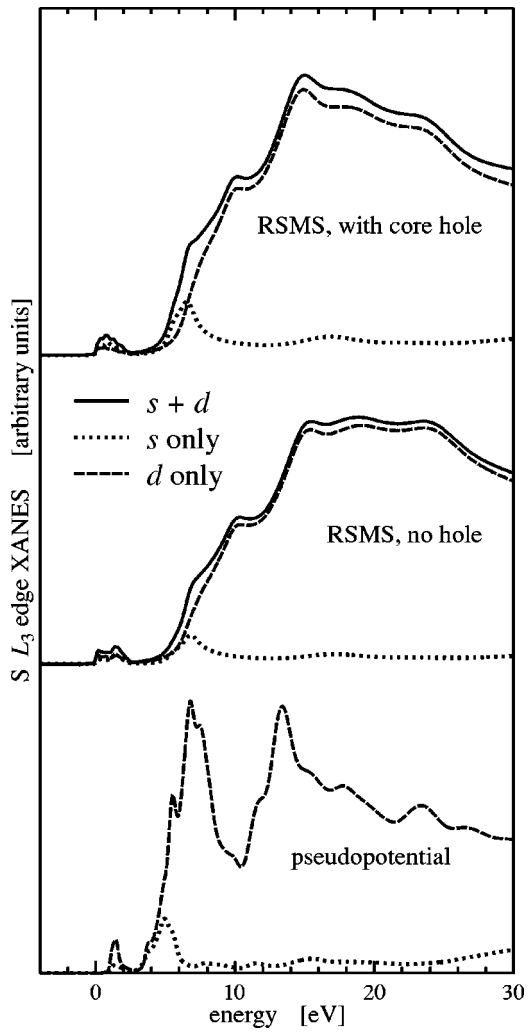

FIG. 3. Theoretical S L_3-edge XANES of $CuFeS_2$ as obtained from RSMS calculations with a $2p$ core hole included, from RSMS calculations neglecting the core hole, and from pseudopotential calculations. Different line types stand for contributions from different angular-momentum channels (*s*, *d*, or both).

The energy dependence of PEPD averaged around selected atoms $P^{(j)}$ is displayed in Figs. 4–6. The PEPD curves were smeared by the same Lorentzian and Gaussian curves as the calculated XANES spectra, so that the XANES and PEPD features can be more easily compared. For each spectrum, the probability densities around only few atoms are displayed in Figs. 4–6 so that the graphs remain legible. In the pre-peak energy region (-5 eV$<E<$6.5 eV), all PEPD curves are scaled down by a factor of 100 so that they fit into the same drawing.

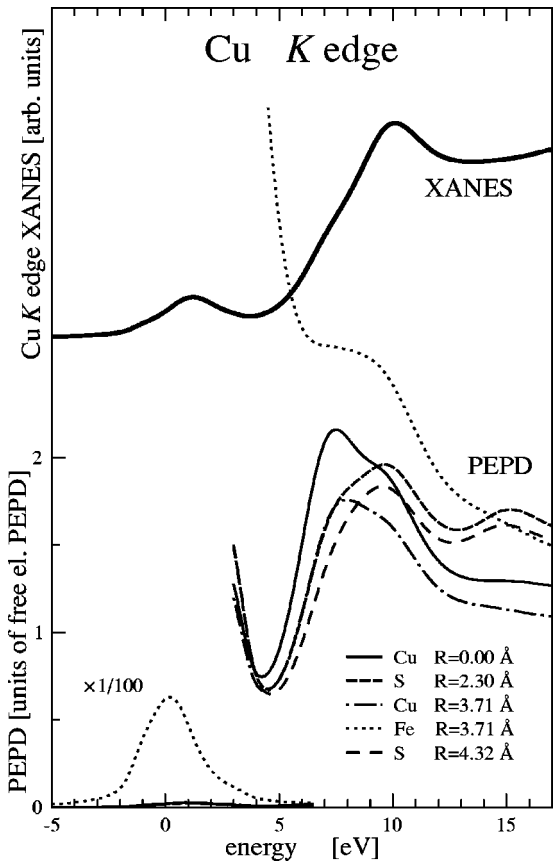

FIG. 4. Photoelectron probability densities around selected atomic sites (lower panel, thin lines) associated with the Cu *K*-edge XANES (upper panel, thick line). The atomic sites are identified in the legend by their chemical types and distances *R* from the center of the 147-atom cluster. In the pre-peak region, the PEPD curves were scaled down by a factor of 100.

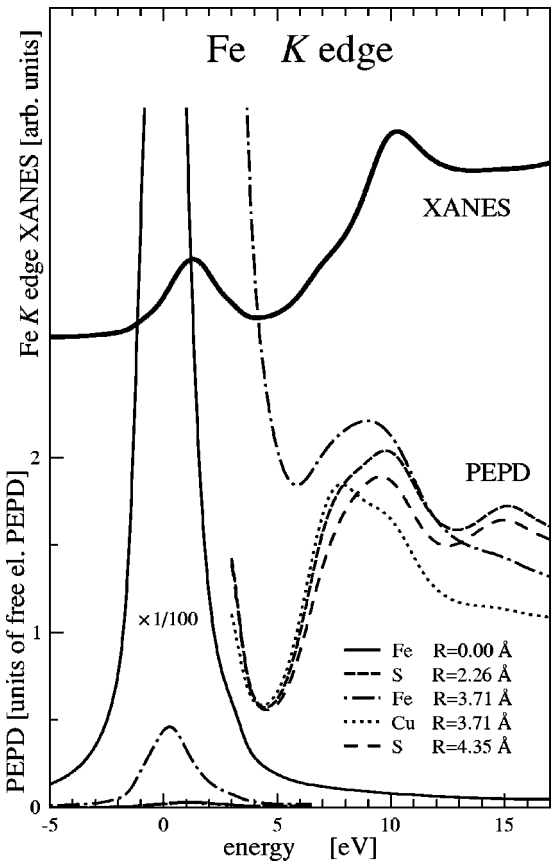

FIG. 5. Photoelectron probability densities around selected atomic sites associated with the Fe *K*-edge XANES. See Fig. 4 for a more detailed description.

As it was found and discussed in previous studies,[31,45] the shape of PEPD curves does not simply copy the XANES spectrum. This is due to the fact that PEPD and XAS carry a different kind of information: While the spectral intensity informs us about the probability that the ejected electron goes anywhere, PEPD tells us how this ''anywhere'' looks like. Only a tiny fraction of the photoelectron density matrix, namely, that part of it which overlaps with the core of the central atom and which has the angular-momentum character conforming to the selection rules, enters indirectly into expressions for the XAS intensity. One can also interpret the lack of simple correspondence between XANES and PEPD peaks as a manifestation of the interference nature of XAS spectral features—they are generated not just through accumulating electrons here and there but rather by interference between many scattering paths.

There is no dramatic dependence of the site-related probabilities $P^{(j)}$ either on the chemical type of the jth atom or on its distance from the center of the cluster, *except for the pre-peak*, where the photoelectron PEPD around Fe atoms is by orders of magnitude larger than around Cu or S atoms. The dominance of Fe atoms in the pre-edge region is so overwhelming that it even spills to the main-peak region (around $E \approx 7-12$ eV) by means of the Lorentzian and Gaussian broadening. This can be nicely illustrated, e.g., in the case of the dotted line in Fig. 4, corresponding to Fe atoms at the distance of $R = 3.71$ Å from the center: the PEPD in the main-peak region has been greatly enhanced by the presence of a huge pre-peak spike nearby, so that this curve even reaches out of the plot for $E \lesssim 5$ eV. For PEPD around the central Fe atom in the case of the Fe *K* edge and around the nearest Fe atom (at $R = 2.26$ Å) in the case of the S *K* edge, this smearing-induced enhancement of the corresponding curves is so large that they even cannot be displayed in the normal scale of the graphs and hence are completely omitted in the main-peak energy region (the full line in Fig. 5 and the short-dashed line in Fig. 6 are missing in the $E > 3$ eV parts of the plots; they are displayed in the scaled-down gauge only instead). This high intensity of Fe-related curves in the main-peak region is, nevertheless, just a technical artifact stemming from our displaying of the *broadened* PEPD curves; the bare (nonconvoluted) PEPD around the Fe sites is not larger than PEPD around the Cu or S sites in the main-peak energy region ($E \approx 7-12$ eV).

It is evident from Figs. 4–6 that the PEPD analysis is especially potent in the pre-peak region, where the differences in PEPD around different atoms may be very large. In order to offer a more complex view on the role played by different atoms at this energy region, we summarize in Tables II–IV the integrals of PEPD curves over the pre-peak

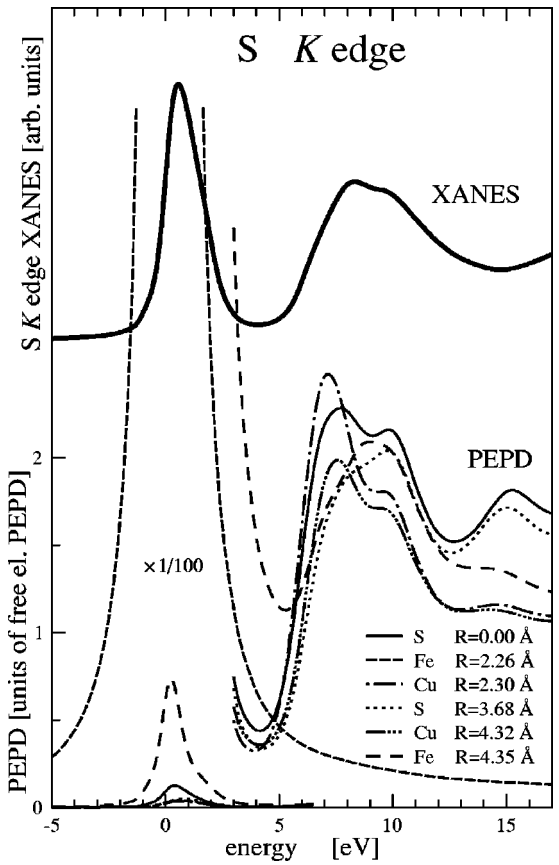

FIG. 6. Photoelectron probability densities around selected atomic sites associated with the S *K*-edge XANES. See Fig. 4 for a more detailed description.

region for all atoms lying within 4.5 Å from the photoabsorbing atom. The PEPD integration interval stretches from 0 to 2.5 eV on the scale of Figs. 4–6, meaning that, e.g., for a free electron this integral would be 2.5 due to the PEPD normalization to the free-electron probability density (cf. Sec. II C). Moreover, we show also the relative differential probability density $q^{(j)}_{\mathrm{DOS}}$ as defined by Eq. (9), integrated over the same energy interval. These two quantities are related in such a way that while the energy-integrated $P^{(j)}$ can be viewed as the probability that a photoelectron ejected during the formation of the pre-peak will be found in the vicinity of the respective atom, the energy-integrated $q^{(j)}_{\mathrm{DOS}}$ may be viewed as a measure of what percentage of this probability is caused by specific XAS-related effects.

The PEPD analysis of the S L_3-edge spectrum yields values very similar to the case of the S *K* edge—a summarizing table analogous to Table IV would contain values differing by not more than 20% from the corresponding values for the S *K* edge. Therefore, we do not show the S L_3-edge results here explicitly, just noting that the conclusions concerning the localization of XAS-related photoelectrons which we draw for the S *K*-edge spectrum remain valid for the S L_3 edge as well.

Tables II–IV show that the site-related photoelectron probability density depends on the size of the cluster. That is not entirely surprising as the PEPD is to a large extent determined by the local DOS, which depends in the size of the cluster.[55] However, no matter what cluster size one employs, the probability density $P^{(j)}$ around the Fe sites is always at least by an order of magnitude larger than $P^{(j)}$ around the Cu or S sites in the pre-peak energy region. In other words, while the details of PEPD distribution depend on the cluster size, its gross features do not. Interestingly, the relative differential probability $q^{(j)}_{\mathrm{DOS}}$ exhibits a significantly larger dependence on the cluster size than the total probability $P^{(j)}$. This probably relates with the fact that $q^{(j)}_{\mathrm{DOS}}$ reflects more subtle effects than $P^{(j)}$. Nevertheless, for both cluster sizes the ratio $q^{(j)}_{\mathrm{DOS}}$ stays in the same order of magnitude, giving thus a rough idea what percentage of photoelectron density is typically conditioned by the x-ray-absorption process itself. One can also observe that $q^{(j)}_{\mathrm{DOS}}$ is ordinarily largest for the photoabsorbing atom and smaller for more distant atoms.

As the total probability density $P^{(j)}$ incorporates the effects of DOS, it does not approach unity (i.e., its free-electron value) with increasing distance of the jth sphere from the center of the cluster. On the other hand, one can presume that $P(\boldsymbol{r})$ would approach $P_{\mathrm{DOS}}(\boldsymbol{r})$ when moving away from the photoabsorbing atom, meaning that the differential probability $q^{(j)}_{\mathrm{DOS}}$ would approach zero eventually. We found that for the outermost atoms of the 207-atom clusters

TABLE II. The photoelectron probability density integrated over the Cu *K*-edge XANES pre-peak energy region (stretching from 0 to 2.5 eV) around atoms in the nearest neighborhood of the photoabsorbing Cu atom. The energy-integrated total PEPD $P^{(j)}$ is in units of free-electron probability density multiplied by 1 eV, the energy-integrated relative differential PEPD $q^{(j)}_{\mathrm{DOS}}$ is in eV. Two cluster sizes of 147 and of 207 atoms are considered (cf. Fig. 4 to view some of the corresponding $P^{(j)}$ curves for the 147-atom cluster).

Distance from center [Å]	Chemical type	No. of atoms in the shell	Total PEPD $P^{(j)}$ 147 atoms	Total PEPD $P^{(j)}$ 207 atoms	Relative differential PEPD $q^{(j)}_{\mathrm{DOS}}$ 147 atoms	Relative differential PEPD $q^{(j)}_{\mathrm{DOS}}$ 207 atoms
0.00	Cu	1	4.2	4.1	0.163	0.167
2.30	S	4	4.5	3.2	0.120	0.102
3.71	Cu	4	4.2	3.9	0.070	0.067
3.71	Fe	4	75.2	90.8	0.065	0.083
3.74	Fe	4	69.2	105.1	0.063	0.119
4.32	S	8	4.1	3.6	0.057	0.032
4.39	S	4	3.9	3.7	0.039	0.038

TABLE III. The photoelectron probability density integrated over the Fe *K*-edge XANES pre-peak energy region around atoms in the nearest neighborhood of the photoabsorbing Fe atom. See Table II for a more detailed caption.

Distance from center [Å]	Chemical type	No. of atoms in the shell	Total PEPD $P^{(j)}$ 147 atoms	Total PEPD $P^{(j)}$ 207 atoms	Relative differential PEPD $q^{(j)}_{\mathrm{DOS}}$ 147 atoms	Relative differential PEPD $q^{(j)}_{\mathrm{DOS}}$ 207 atoms
0.00	Fe	1	899.8	4200.7	0.109	0.187
2.26	S	4	4.2	4.0	0.173	0.114
3.71	Cu	4	4.8	4.8	0.122	0.054
3.71	Fe	4	54.5	99.3	0.072	0.146
3.74	Cu	4	4.5	4.9	0.073	0.067
4.35	S	4	4.1	4.2	0.098	0.049
4.37	S	4	4.1	4.4	0.060	0.056
4.42	S	4	3.8	3.8	0.045	0.039

(at 9.8 Å from the center), typical values of $q^{(j)}_{\mathrm{DOS}}$ are around 0.05 for Fe atoms, meaning that the DOS-like limit has not been reached for this cluster size yet. We did not investigate this issue further as it would be computationally quite demanding and it is not directly relevant to our topic.

Generally, there appears to be no simple pattern in the spatial dependence of the photoelectron PEPD: the site-related probabilities do not monotonously depend on the distance from the center or on the symmetry of atomic sites. It seems that the spatial localization of photoelectrons associated with particular spectral peaks cannot be just ''guessed'' by means of any simple rule of thumb.

A firm conclusion can be drawn from the total $P^{(j)}$ curves in Figs. 4–6 and from their integrals in Tables II–IV that the pre-peak photoelectron states are almost exclusively located on Fe atoms. It was suggested earlier already[21–23] that these states are derived from the $3d$ states of Fe. Discrete variational $X\alpha$ calculations of Hamajima *et al.*[56] as well as our own SCF-$X\alpha$ molecular calculations confirm this. Hence, in this sense one could indeed speak about an *atomiclike* character of the pre-peak. On the other hand, it is obvious that these states are actually spatially extended, resting practically on all the Fe atoms contained in the cluster (we checked that the dominance of Fe over Cu and S as concerns $P^{(j)}$ is not restricted to atoms close to the photoabsorbing one). Hence one can rightfully interpret the pre-peak states as being multiple-scattering resonances, i.e., arising from interference effects of the photoelectron wave function from the crystal structure.[24] Both interpretations of the XANES pre-peak in $CuFeS_2$ can thus be unified within the single framework of PEPD analysis.

In contrast to the total probability density $P^{(j)}$, the relative differential probability density $q^{(j)}_{\mathrm{DOS}}$ does not exhibit any drastic dependence on the chemical type of the jth atom (last two columns in Tables II–IV), neither does it vary too much from site to site. As $q^{(j)}_{\mathrm{DOS}}$ is a measure how the photoelectron is specifically affected by the x-ray-absorption process, this fact can be viewed as a manifestation that the XANES fine structure is not conditioned on just a few atoms and/or scattering paths; rather, it arises from subtle adding and subtract-

TABLE IV. The photoelectron probability density integrated over the S *K*-edge XANES pre-peak energy region around atoms in the nearest neighborhood of the photoabsorbing S atom. See Table II for a more detailed caption.

Distance from center [Å]	Chemical type	No. of atoms in the shell	Total PEPD $P^{(j)}$ 147 atoms	Total PEPD $P^{(j)}$ 207 atoms	Relative differential PEPD $q^{(j)}_{\mathrm{DOS}}$ 147 atoms	Relative differential PEPD $q^{(j)}_{\mathrm{DOS}}$ 207 atoms
0.00	S	1	13.1	13.1	0.342	0.334
2.26	Fe	2	4238.0	7808.1	0.158	0.271
2.30	Cu	2	4.0	4.0	0.204	0.194
3.68	S	2	4.5	4.5	0.213	0.188
3.68	S	4	4.8	4.1	0.228	0.189
3.74	S	4	3.6	3.3	0.177	0.177
3.80	S	2	3.1	3.2	0.177	0.167
4.32	Cu	4	4.4	4.4	0.191	0.171
4.34	Cu	2	4.3	4.4	0.175	0.158
4.35	Fe	4	70.2	74.7	0.135	0.159
4.37	Fe	2	66.0	152.2	0.181	0.177
4.39	Cu	2	4.4	4.4	0.169	0.136
4.42	Fe	2	86.1	112.8	0.101	0.126

ing of many terms, neither of which can be singled out as the most important one. Indeed, the effects of hundreds or thousands of scattering paths have to be summed together in order to yield the desired XANES spectrum in the scattering path summation approach.[57]

As a whole, Tables II–IV indicate that while the pre-peak photoelectrons are located predominantly on Fe atoms, specific XAS-related influence on the photoelectron probability distribution can be observed around other atoms as well. One can expect, therefore, that other than iron atoms will have their role in creating the pre-peak as well. This will be elaborated more deeply in the following section.

Finally, let us note that our finding that the peak-forming photoelectron states are confined nearly exclusively to the Fe sites has a counterpart in an earlier investigation of a TiS_2 spectrum:[31] it was found by analyzing the total probability $P^{(j)}$ that the states responsible for the pre-peak at the Ti *K*-edge XANES of TiS_2 are located predominantly on Ti atoms, practically avoiding the sulphurs. On the other hand, the differential probability $P^{(j)}-P^{(j)}_{\mathrm{DOS}}$ was found to be quite large around the nearest S atoms.[31] One can thus conjecture that in transition-metal compounds, the pre-peak states are generally located at the transition-metal atoms, while specific XAS-related effects as quantified by $q^{(j)}_{\mathrm{DOS}}$ can be observed at atoms of other chemical species as well.

D. Cluster size effect

The role of various atoms in forming XANES peaks has been often assessed by means of a theoretical exploration of the cluster size effect. To connect between this procedure and the PEPD analysis, we study in this section the influence of the size of the cluster involved in the RSMS calculation on the Cu, Fe, and S *K*-edge spectra. Our results are summarized in Fig. 7 (a potential that accounts for the 1*s* core hole was employed). In order to present a more complete picture, both unsmeared and convoluted theoretical curves are displayed in this figure.

In the case of the Cu *K*-edge spectrum, there appears to be a correspondence between the importance of individual atoms as inferred from the cluster size effect and the probability $P^{(j)}$ that the pre-peak photoelectron is located near these atoms: the pre-peak emerges only after Fe atoms have been included in the cluster, i.e., if its size reaches 13 atoms. A similar situation occurs for the S *K*-edge XANES, where just a three-atom cluster (comprising one S and two Fe atoms) is sufficient to generate the pre-peak. A different situation arises for the Fe *K* edge: the $P^{(j)}$ probabilities of Table III show that the photoelectron rests practically only on the central Fe atom while Fig. 7 clearly shows that the presence of the central atom alone is not enough for the pre-peak to be formed, despite the fact that this atom completely dominates the $P^{(j)}$ spatial distribution. This disproportion can be, nevertheless, understood intuitively given the fact that the photoelectron states resting on the central Fe have almost exclusively a *d* character and hence *cannot be accessed directly* by a dipole transition from the 1*s* core state. Only after the neighboring atoms are accounted for, the symmetry is lowered and a *p* character is introduced into the lowest unoccupied states. In the language of multiple-scattering formalism, one can view this even more intuitively by imagining that the core electron is initially excited into a pure *p* state via the dipole rule but it is scattered off the neighbors thereafter and reapproaches the photoabsorbing atom in such a way that its wave function now has a sizable *d* component with respect to its center. Obviously, one may not take this intuitive picture too literally—-the multiple-scattering formalism employed in this paper describes a stationary situation, not a time evolution.

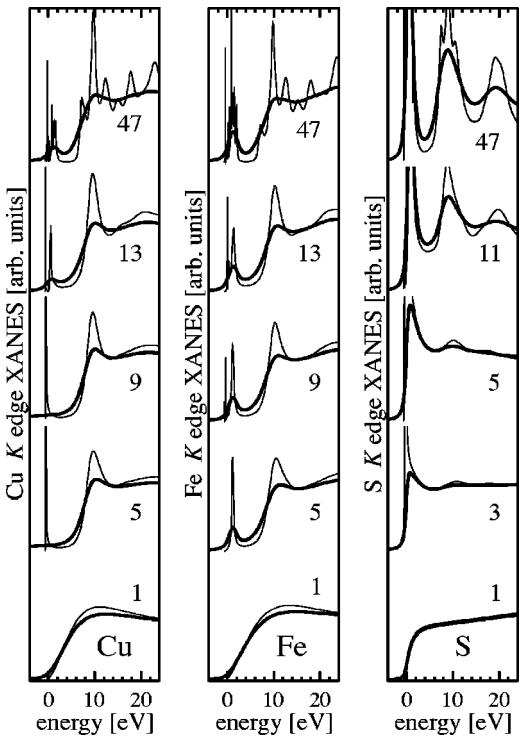

FIG. 7. Cu, Fe, and S *K*-edge XANES of $CuFeS_2$ obtained via RSMS calculations for different cluster sizes (indicated by the numbers of atoms at each curve). Thick curves stand for broadened spectra, thin lines display raw theoretical results.

The Fe *K*-edge pre-peak may thus serve as an example of a situation where in spite of the photoelectron being practically located on a single atom, that single atom still is not able to reproduce the relevant spectral peak alone. Similarly, a concurrent analysis of the site-related probabilities $P^{(j)}$ and of the cluster size effect at the Fe *K*-edge pre-peak illustrates that negligibility of photoelectron probability density around a certain atom does not imply that this atom is not important for forming the XANES. E.g., the S atoms nearest to the central Fe are essential for forming the pre-peak (middle panel of Fig. 7) and yet the probability that the pre-peak-related photoelectron will be found in the vicinity of these S atoms is by orders of magnitude smaller than the probability that it will be found at the central Fe (Table III). On the other hand, the DOS-subtracted relative probability $q^{(j)}_{\mathrm{DOS}}$ is quite high at the S atoms, suggesting thus beforehand that these atoms may play an important role in creating the pre-peak. Similarly as in our earlier study of TiS_2 (Ref. 31), we thus observe that the differential probability $P(\boldsymbol{r})-P_{\mathrm{DOS}}(\boldsymbol{r})$

seems to be a better measure of importance of particular atoms for creating XANES peaks than the bare probability $P(\boldsymbol{r})$ itself.

Our study demonstrates that the spatial localization of pre-peak states cannot be properly estimated by a mere inspection of the influence of these atoms on the creation of this pre-peak. Conversely, neither the relative importance of various atoms for creating the pre-peak can be inferred just from comparing the photoelectron probability densities $P^{(j)}$ associated with them. Analyzing PEPD and exploring the cluster size effect are, nevertheless, rather complementary than conflicting approaches to understanding XANES. The quantum-mechanical probability density $P(\boldsymbol{r})$ is a well-defined quantity and answers the question about localization of the XANES photoelectron. Importance of individual atoms for creating a XANES peak is an empirical and somewhat ambiguous quantity and answers the question about influence of the photoelectron on peak formation. Both methods ought to be combined in order to facilitate a comprehensive understanding of XANES features.

IV. CONCLUSIONS

By exploring the photoelectron probability densities, we found that the pre-peak at the Cu, Fe, and S *K*-edge XANES of $CuFeS_2$ is formed by transitions of the excited photoelectron into states localized mainly at all the Fe sites (not just those Fe sites which are most close to the photoabsorbing atom). Two intuitive views of the pre-peak, namely, an atomistic interpretation stressing the local aspect and a multiple-scattering interpretation stressing the extended nature of the photoelectron, can thus be included into a single scheme.

ACKNOWLEDGMENTS

The research work at the Institute of Physics was carried out within the program ''Experimental and theoretical research of condensed systems'' under the Project No. AVOZ-010-914. The work on chalcopyrite structures was supported by Grant No. 202/02/0841 of the Grant Agency of the Czech Republic.

[1] P. Kizler, P. Lamparter, and S. Steeb, Z. Naturforsch., A: Phys. Sci. **44a**, 189 (1989); P. Kizler, Phys. Rev. Lett. **67**, 3555 (1991); P. Kizler, Phys. Rev. B **48**, 12 488 (1993).

[2] F. Farges, G.E. Brown, Jr., and J.J. Rehr, Geochim. Cosmochim. Acta **60**, 3023 (1996); F. Farges, G.E. Brown, Jr., and J.J. Rehr, Phys. Rev. B **56**, 1809 (1997).

[3] S. Della Longa, A. Arcovito, M. Girasole, J.L. Hazemann, and M. Benfatto, Phys. Rev. Lett. **87**, 155501 (2001); M. Benfatto, S. Della Longa, and C.R. Natoli, J. Synchrotron Radiat. **10**, 51 (2003).

[4] L.A. Bugaev, A.P. Sokolenko, H.V. Dmitrienko, and A.-M. Flank, Phys. Rev. B **65**, 024105 (2001).

[5] O. Šipr, G. Dalba, and F. Rocca, Phys. Chem. Glasses **44**, 252 (2003).

[6] R.V. Vedrinskii, V.L. Kraizman, A.A. Novakovich, Ph.V. Demekhin, and S.V. Urazhdin, J. Phys.: Condens. Matter **10**, 9561 (1998).

[7] O. Šipr, A. Šimůnek, S. Bocharov, Th. Kirchner, and G. Dräger, Phys. Rev. B **60**, 14 115 (1999).

[8] A. Gloter, J. Ingrin, D. Bouchet, and C. Colliex, Phys. Rev. B **61**, 2587 (2000).

[9] Q. Qian, T.A. Tyson, C.C. Kao, M. Croft, S.W. Cheong, G. Popov, and M. Greenblatt, Phys. Rev. B **64**, 024430 (2001).

[10] Z.Y. Wu, C.R. Natoli, A. Marcelli, E. Paris, F. Seifert, J. Zhang, and T. Liu, J. Synchrotron Radiat. **8**, 215 (2001).

[11] G. Pfeiffer, J.J. Rehr, and D.E. Sayers, Phys. Rev. B **51**, 804 (1995); G. Pfeiffer, J.J. Rehr, and D.E. Sayers, Physica B **209**, 385 (1995).

[12] S.P. Farrell and M.E. Fleet, Solid State Commun. **113**, 69 (2000).

[13] A. Agui, J.-H. Guo, C. Såthe, J. Nordgren, M. Hidaka, and I. Yamada, Solid State Commun. **118**, 619 (2001).

[14] J. Danger, P. Le Févre, H. Magnan, D. Chandesris, S. Bourgeois, J. Jupille, T. Eickhoff, and W. Drube, Phys. Rev. Lett. **88**, 243001 (2002).

[15] Y. Wu and D.E. Ellis, J. Phys.: Condens. Matter **7**, 3973 (1995).

[16] Z.Y. Wu, G. Ouvrard, P. Moreau, and C.R. Natoli, Phys. Rev. B **55**, 9508 (1997).

[17] F. Bridges, C.H. Booth, M. Anderson, G.H. Kwei, J.J. Neumeier, J. Snyder, J. Mitchell, J.S. Gardner, and E. Brosha, Phys. Rev. B **63**, 214405 (2001).

[18] Z.Y. Wu, C.R. Natoli, A. Marcelli, E. Paris, A. Bianconi, and N. L. Saini, in *Proceedings of the 19th International Conference on X-Ray and Inner-Shell Processes, Rome, 2002*, edited by A. Bianconi, A. Marcelli, and N.L. Saini (Springer, Heidelberg, 2003).

[19] S.M. Butorin, J.H. Guo, L.C. Duda, N. Wassdahl, J. Nordgren, E.Z. Kurmaev, and S.P. Tolochko, Physica C **235**, 1047 (1994).

[20] R.V. Vedrinskii, V.L. Kraizman, A.A. Novakovich, Sh.M. Elyafi, S. Bocharov, Th. Kirchner, and G. Dräger, Phys. Status Solidi B **226**, 203 (2001).

[21] J. Petiau, Ph. Sainctavit, and G. Calas, Mater. Sci. Eng., B **1**, 237 (1988).

[22] Ph. Sainctavit, J. Petiau, A.M. Flank, J. Ringeissen, and S. Lewonczuk, Physica B **158**, 623 (1989).

[23] D. Li, G.M. Bancroft, M. Kasrai, M.E. Fleet, B.X. Yang, X.H. Feng, K. Tan, and Mingsheng Peng, Phys. Chem. Miner. **20**, 489 (1994).

[24] D.A. McKeown, Phys. Rev. B **45**, 2648 (1992).

[25] J.E. Jaffe and A. Zunger, Phys. Rev. B **28**, 5822 (1983).

[26] O. Šipr, P. Machek, A. Šimůnek, J. Vackář, and J. Horák, Phys. Rev. B **56**, 13 151 (1997).

[27] R. Bacewicz, A. Wolska, K. Lawniczak-Jablonska, and Ph. Sainctavit, J. Phys.: Condens. Matter **12**, 7371 (2000).

[28] A.A. Lavrentyev, I.Ya. Nikiforov, and B.V. Gabrelian, J. Phys. IV **7**, C2 (1997); A.A. Lavrentyev, B.V. Gabrelian, V.A. Dubeiko, I.Ya. Nikiforov, and J.J. Rehr, J. Phys. Chem. Solids **63**, 227 (2002); A.A. Lavrentyev, B.V. Gabrelian, I.Ya. Nikiforov, J.J. Rehr, and A.L. Ankudinov, Physca Scr. (to be published).

[29] J.E. Jaffe and A. Zunger, Phys. Rev. B **30**, 741 (1984).

[30] O. Šipr, J. Drahokoupil, P. Machek, and A. Šimůnek, Physca Scr. (to be published).
[31] O. Šipr, Phys. Rev. B **65**, 205115 (2002).
[32] D.D. Vvedensky, in *Unoccupied Electronic States*, edited by J.C. Fuggle and J.E. Inglesfield (Springer, Berlin, 1992), p. 139.
[33] C.R. Natoli, M. Benfatto, S. Della Longa, and K. Hatada, J. Synchrotron Radiat. **10**, 26 (2003).
[34] D.D. Vvedensky, D.K. Saldin, and J.B. Pendry, Comput. Phys. Commun. **40**, 421 (1986).
[35] O. Šipr, computer code RSMS (Institute of Physics AS CR, Prague, 1996).
[36] K.H. Johnsson, Adv. Quantum Chem. **7**, 143 (1973).
[37] M. Cook and D.A. Case, computer code XASCF (Quantum Chemistry Program Exchange, Indiana University, Bloomington, Indiana, 1980).
[38] O. Sipr and A. Šimůnek, J. Phys.: Condens. Matter **13**, 8519 (2001).
[39] J. Vackář, M. Hyt'ha, and A. Šimůnek, Phys. Rev. B **58**, 12 712 (1998).
[40] A. Šimůnek, J. Vackář, M. Polčík, J. Drahokoupil, W. Wolf, and R. Podloucky, Phys. Rev. B **61**, 4385 (2000).
[41] See, e.g., W.E. Pickett, Comput. Phys. Rep. **9**, 115 (1989).
[42] A. Šimůnek, M. Polčík, and G. Wiech, Phys. Rev. B **52**, 11 865 (1995).
[43] F. Al Shamma, M. Abbate, and J.C. Fuggle, in *Unoccupied Electron States*, edited by J.C. Fuggle and J.E. Inglesfield (Springer, Berlin, 1992), p. 347.
[44] J.E. Müller, O. Jepsen, and J.W. Wilkins, Solid State Commun. **42**, 365 (1982).
[45] O. Šipr, J. Synchrotron Radiat. **8**, 232 (232).
[46] O. Šipr, J. Phys.: Condens. Matter **13**, 8519 (2001).
[47] P.J.W. Weijs *et al.*, Phys. Rev. B **41**, 11 899 (1990).
[48] F. Rapisarda and O. Bisi, Phys. Rev. B **47**, 13 914 (1993).
[49] T. Mizoguchi, I. Tanaka, M. Yoshiya, F. Oba, K. Ogasawara, and H. Adachi, Phys. Rev. B **61**, 2180 (2000).
[50] S.-D. Mo and W.Y. Ching, Phys. Rev. B **62**, 7901 (2000).
[51] K. Kokko, V. Kulmala, and J.A. Leiro, Phys. Rev. B **66**, 165114 (2002).
[52] M. Cardona and L. Ley, *Photoemission in Solids I: General Principles* (Springer-Verlag, Berlin, 1978).
[53] J. Chaboy, Solid State Commun. **99**, 877 (1996).
[54] H. Ebert, J. Stöhr, S.S.P. Parkin, M. Samant, and A. Nilsson, Phys. Rev. B **53**, 16 067 (1996).
[55] O. Šipr, J. Phys.: Condens. Matter **13**, 4291 (2001).
[56] T. Hamajima, T. Kambara, K.I. Gondaira, and T. Oguchi, Phys. Rev. B **24**, 3349 (1981).
[57] S.I. Zabinsky, J.J. Rehr, A. Ankudinov, R.C. Albers, and M.J. Eller, Phys. Rev. B **52**, 2995 (1995); J.J. Rehr and R.C. Albers, Rev. Mod. Phys. **72**, 621 (2000).